REPORT DOCUMEN

AD-A279 700

Form Approved
OMB No 0704-0188

(1)

1. AGENCY USE ONLY (Leave blank)	2. REPORT DATE	3. REPORT TYPE AND DATES COVERED
	6 May 1994	Technical Report

4. TITLE AND SUBTITLE
Gas-Phase Generation of Zinc Sulfide Particles Using a Single-Source Precursor

5. FUNDING NUMBERS
N00014-91-J-1258
Matlsyn---01

6. AUTHOR(S)
D. Zeng, M. J. Hampden-Smith, and A. Datye, Q. Powell, A. Gurav and T. Kodas.

7. PERFORMING ORGANIZATION NAME(S) AND ADDRESS(ES)
Departments of Chemistry and Chemical Engineering
Center for Micro-Engineered Ceramics
University of New Mexico
Albuquerque, NM 87131

8. PERFORMING ORGANIZATION REPORT NUMBER
Technical Report No. 13

9. SPONSORING/MONITORING AGENCY NAME(S) AND ADDRESS(ES)
Dr. H. Guard and Dr. L. Kabikoff
Office of Naval Research
800 North Quincy Street
Arlington, VA 22217-5000

10. SPONSORING/MONITORING AGENCY REPORT NUMBER

11. SUPPLEMENTARY NOTES
Submitted to Chemistry of Materials

12a. DISTRIBUTION/AVAILABILITY STATEMENT
Approval for public release; distribution unlimited

12b. DISTRIBUTION CODE
N00179

13. ABSTRACT (Maximum 200 words)

Nanometer-sized (20 to 40 nm) ZnS particles were produced in a flow reactor by gas-phase reaction of the single-source precursor $Zn(S_2CNEt_2)_2(TMEDA)$, where TMEDA = tetramethylethylenediamine. The precursor was prepared by reaction of the dimer, $[Zn(S_2CNEt_2)_2]_2$, with two equivalents of TMEDA. The product was isolated in quantitative yield and characterized by a variety of spectroscopic techniques and by single-crystal X-ray diffraction in the solid state. Transparent, colorless prisms of empirical formula $C_{16}H_{36}N_4S_4Zn$ crystallized by cooling a warm (60°C), saturated toluene solution to room temperature, in the orthorhombic crystal system, space group $P2_12_12_1$ with unit cell dimensions a = 8.785(1) Å, b = 11.611(2) Å, c = 23.321(2) Å, z = 4, with R = 4.64%, R_W = 5.32% for 3262 independent reflections where $F > 3.0\,\sigma(F)$. The structure of $Zn(S_2CNEt_2)_2(TMEDA)$ was monomeric and distorted octahedral in the solid state. The precursor was evaporated into the gas phase and reacted in a hot-wall reactor at temperatures of 500, 600, and 700° C resulting in the formation of ZnS particles X-ray diffraction showed phase-pure ZnS particles with crystallite sizes of 15 - 25 nm at all temperatures studied. Thermo-gravimeteric analysis, elemental analysis, and transmission electron microscopy suggested that the particles also contained sulfur derived from the precursor.

14. SUBJECT TERMS			15. NUMBER OF PAGES
			16. PRICE CODE
17. SECURITY CLASSIFICATION OF REPORT	18. SECURITY CLASSIFICATION OF THIS PAGE	19. SECURITY CLASSIFICATION OF ABSTRACT	20. LIMITATION OF ABSTRACT
Unclassified	Unclassified	Unclassified	

OFFICE OF NAVAL RESEARCH

GRANT N00014-91-J-1258

R&T Code Matlsyn---01

Technical Report #13

Gas-Phase Generation of Zinc Sulfide Particles Using a Single-Source Precursor

by

D. Zeng, A. Datye, Q. Powell, T. T. Kodas
A. Gurav and M. J. Hampden-Smith

Prepared for Publication in

Chemistry of Materials

Department of Chemistry and Center for Micro-Engineered Ceramics
University of New Mexico
Albuquerque, NM 87131.

Gas-Phase Generation of Zinc Sulfide Particles Using a Single-Source Precursor

Q. Powell, A. Gurav, T. Kodas*

Department of Chemical Engineering and Center For Micro-Engineered Ceramics

University of New Mexico

Albuquerque, NM 87131

M.J. Hampden-Smith* and D. Zeng

Department of Chemistry and Center For Micro-Engineered Ceramics

University of New Mexico

Albuquerque, NM 87131

L. M. Wang

Department of Geology

University of New Mexico

Albuquerque, NM 87131

*Authors to whom correspondence should be addressed.

Submitted to Chemistry of Materials

Abstract

Nanometer-sized (20 to 40 nm) ZnS particles were produced in a flow reactor by gas-phase reaction of the single-source precursor $Zn(S_2CNEt_2)_2(TMEDA)$, where TMEDA = tetramethylethylenediamine. The precursor was prepared by reaction of the dimer, $[Zn(S_2CNEt_2)_2]_2$, with two equivalents of TMEDA. The product was isolated in quantitative yield and characterized by a variety of spectroscopic techniques and by single-crystal X-ray diffraction in the solid state. Transparent, colorless prisms of empirical formula $C_{16}H_{36}N_4S_4Zn$ crystallized by cooling a warm (60 °C), saturated toluene solution to room temperature, in the orthorhombic crystal system, space group $P2_12_12_1$ with unit cell dimensions a = 8.785(1) Å, b = 11.611(2) Å, c = 23.321(2) Å, z = 4, with R = 4.64%, R_w = 5.32% for 3262 independent reflections where $F > 3.0\ \sigma(F)$. The structure of $Zn(S_2CNEt_2)_2(TMEDA)$ was monomeric and distorted octahedral in the solid state. The precursor was evaporated into the gas phase and reacted in a hot-wall reactor at temperatures of 500, 600, and 700 °C resulting in the formation of ZnS particles. X-ray diffraction showed phase-pure ZnS particles with crystallite sizes of 15 - 25 nm at all temperatures studied. Thermo-gravimeteric analysis, elemental analysis, and transmission electron microscopy suggested that the particles also contained sulfur derived from the precursor.

Introduction

The generation of nanometer-scale semiconducting materials is an area of intense current interest because they exhibit unusual reactivity and electronic and optical properties which may be exploited for a variety of applications.[1-5] There are several liquid-phase approaches that are capable of making particles with diameters in the nanometer size range.[6-8] Gas-phase methods have also demonstrated this capability,[9-11] but only a few semiconducting materials including silicon, GaAs, and CdS have been produced.[9,12-16]

A key problem for gas-phase routes is generation of nanometer-sized multicomponent particles with controlled stoichiometries. Poor control over final particle stoichiometry in binary and ternary materials can occur when two or more gaseous reagents are used as precursors. In many cases, chemically inhomogeneous products result as shown in Figure 1. Several factors contribute to this problem. The vaporization rates of the individual precursors may vary with time leading to changes in their relative concentrations. The reaction rates of the individual compounds vary independently as a function of temperature leading to difficulties in controlling the relative extent of reaction of the separate precursors as reaction conditions are varied. The different activation energies for the reactions of the precursors also lead to chemical reactions of the separate precursors at different locations in the reactor because of axial temperature profiles. Finally, the nucleation rates of the reaction products from the gas phase can depend strongly on surface energies. As a result, the reaction products are likely to be formed at different locations in the reactor and lead to nucleation of the individual species. The growth of these species will result in chemically inhomogeneous particles.[17]

FIG. 1

One method for overcoming the problems of inhomogeneity and lack of control over stoichiometry is to use single-source precursors which contain the desired elements in a single molecule. This method has been used in many CVD systems to form films[18-26] but has not been used for aerosol generation of multicomponent materials. Figure 2 demonstrates the advantage of using a single-source precursor for gas-phase particle

FIG 2

formation. The precursor is introduced into the gas phase where chemical reaction occurs to form the product. The concentration of the product increases until the vapor is sufficiently supersaturated to result in particle formation. If the bond(s) holding the desired elements together are not broken during reaction, the stoichiometry of the precursor is preserved in the product.

This paper discusses generation of nanometer-sized zinc sulfide particles by vapor-phase reaction of a single-source volatile precursor. A variety of precursors have been used to prepare ZnS films by CVD including the reactions of dialkyl zinc compounds with *t*-butyl mercaptan[27] and metallic zinc vapor with hydrogen sulfide.[28] These methods suffer from the problems that the precursors are either oligomeric resulting in relatively low vapor pressures, or control over stoichiometry is difficult. In addition, many volatile sulfur precursors such as H_2S are dangerous to handle. More recently, zinc dialkyldithiocarbamates have been shown to thermally decompose to form pure ZnS at relatively low temperatures (400 °C).[29-31] However, species such as $[Zn(S_2CNEt_2)]_2$ and $[MeZn(S_2CNEt_2)_2]_2$ are dimeric in the solid state and, as a result, have rather low volatility.[32,33]

In this work, we have prepared the Lewis base adduct, $Zn(S_2CNEt_2)_2(TMEDA)$, where TMEDA = tetramethylenediamine, in which the degree of aggregation of $[Zn(S_2CNEt_2)_2]_2$ was reduced in the solid state by chelation with TMEDA. This reactant was introduced in the gas-phase into a hot-wall reactor where reaction and particle formation occurred. The synthesis and characterization of $Zn(S_2CNEt_2)_2(TMEDA)$, the reactor design, reaction conditions, and powder characteristics of the ZnS powders formed via this aerosol method are described.

Experimental Section

(i) General Procedures. All manipulations were carried out under an atmosphere of dry nitrogen using standard Schlenk techniques, although the starting materials and products were neither oxidation nor moisture sensitive. All hydrocarbon and ethereal solvents were dried and distilled from sodium benzophenone ketyl and stored over 4 Å molecular sieves under a nitrogen atmosphere prior to use. The reagents $[Zn(S_2CNEt)_2]_2$ and tetramethylethylenediamine, TMEDA, were purchased from Aldrich Chemical Company and used without further purification. Elemental analyses were performed by Ms. R. Ju at the University of New Mexico, Department of Chemistry. NMR data were recorded on a Bruker AC-250P NMR spectrometer using the protio impurities of the deuterated solvents as references for the ^1H NMR and the $^{13}C\{^1H\}$ resonance of the solvents as reference for $^{13}C\{^1H\}$ NMR spectroscopy. Temperatures were calibrated with either ethylene glycol or methanol. IR data were recorded on a Perkin-Elmer Model 1620 FTIR spectrophotometer.

(ii). Synthesis and characterization of $Zn(S_2CNEt_2)_2$(TMEDA). The reagent $[Zn(S_2CNEt_2)_2]_2$, 10g, 0.028 mol. was placed in a 500mL Schlenk flask together with 120 mL of toluene to form a white suspension. On addition of TMEDA, 4.1 mL more of the white solid dissolved to form a pale yellow solution. The total volume of the solution was made up to 200 mL through addition of toluene and on heating to 60 °C for 15 min, all the remaining white solid dissolved. The solution was then set aside to cool to room temperature. After standing for 12hr., 7.7465g, 0.016 mol. of large transparent colorless crystals were isolated. The volume of the solvent was reduced *in vacuo* by approximately half until the product started to precipitate at room temperature. The solution was then warmed to 60 °C to redissolve the white precipitate and was then cooled to -30 °C. A second crop of crystals was obtained, 5.01g, 0.01 mol. to give a combined yield of 12.76g, 0.027 mol., 96%. The crystalline material analyzed correctly for

$Zn(S_2CNEt_2)_2$(TMEDA) and crystals obtained in this way were used for the single-crystal X-ray diffraction study.

$Zn(S_2CNEt_2)_2$(TMEDA): IR (KBr disk, cm^{-1}): 2989 cm^{-1} (m), 2965 cm^{-1} (s), 2930 cm^{-1} (m), 2870 cm^{-1} (s), 2836 cm^{-1} (m), 2793 cm^{-1} (m), 1480 cm^{-1} (vs), 1459 cm^{-1} (vs), 1419 cm^{-1} (vs), 1375 cm^{-1} (m), 1357 cm^{-1} (s), 1303 cm^{-1} (m), 1271 cm^{-1} (vs), 1211 cm^{-1} (s), 1141 cm^{-1} (s), 1091 cm^{-1} (m), 1078 cm^{-1} (m), 1029 cm^{-1} (m), 1013 cm^{-1} (m), 993 cm^{-1} (vs), 952 cm^{-1} (m), 914 cm^{-1} (m), 844 cm^{-1} (m), 792 cm^{-1} (m), 669 cm^{-1} (w), 608 cm^{-1} (w), 567 cm^{-1} (m), 500 cm^{-1} (w), 472 cm^{-1} (w), 437 cm^{-1} (w). ^{1}H-NMR (C_7D_8) at 300K: 1.02 ppm (t, $^3J_{H-H}$ = 7.0 Hz, 12 H, NCH_2CH_3), 2.18 ppm (s, 4 H, Me_2NCH_2), 2.30 ppm [s, 12 H, $(CH_3)_2NCH_2$], 3.59 ppm (q, $^3J_{H-H}$ = 7.1 Hz, 8 H, NCH_2CH_3); at 183K and 173K: 1.03 ppm (s, NCH_2CH3), 2.46 ppm [br, overlapped resonances of Me_2NCH_2 and $(CH_3)_2NCH_2$], 3.45 ppm (d, two types of NCH_2CH_3). ^{13}C-NMR (C_7D_8): 12.30 ppm (s, NCH_2CH_3), 46.18 ppm (s, Me_2NCH_2), 49.08 ppm [s, $(CH_3)_2NCH_2$], 57.03 ppm (s, NCH_2CH_3), 206.01 ppm (s, CS_2-).

$Zn(Et_2NCS_2)_2$: ^{1}H-NMR (C_7D_8) at 283K: 0.83 ppm (t,$^3J_{H-H}$ = 7.1 Hz, 12 H, $NCH_2C\underline{H}_3$), 3.28 ppm (q, $^3J_{H-H}$ = 7.1 Hz, 8 H, $NC\underline{H}_2CH_3$); at 173K: 0.69 ppm (s, $NCH_2C\underline{H}_3$), 2.96 ppm (s, $NC\underline{H}_2CH_3$). ^{13}C-NMR (C_7D_8): 11.93 ppm (s, $NCH_2\underline{C}H_3$), 49.10 ppm (s, $N\underline{C}H_2CH_3$), 203.13 ppm (s, $\underline{C}S_2^-$).

(iii) Single-Crystal X-ray Diffraction data for $Zn(S_2CNEt_2)_2$(TMEDA). Colorless, transparent prisms of $Zn(S_2CNEt_2)_2$(TMEDA) were grown from toluene solution by slowly cooling a saturated solution from 60 °C to room temperature. The crystal data collection and refinement parameters are summarized in Table 1. The crystal TABLE 1 was identified as belonging to the orthorhombic crystal system with space group $P2_12_12_1$. Direct methods yielded the Zn atom position, and the rest of the non-hydrogen atoms were located by full-matrix refinement on the trial model and subsequent interpretation of the difference Fourier maps. The structure was refined with all non-hydrogen atoms isotropic,

followed by all non-hydrogen atoms anisotropic with no hydrogen atoms. The next stage of the refinement included H atoms in idealized positions calculated with a riding model and with fixed isotropic U's set to 1.25 times the isotropic U or U(equivalent) of their parent atoms. The 4 1 0 reflection showed a large ds of 9.7. Inspection of the data collection revealed no obvious error, but elimination of this reflection from the data set gave R = 4.56% and R_w = 5.18%. In the final refinement cycle the non-hydrogen atoms were included as anisotropic and the 4 1 0 refection was included since there was no obvious reason to omit this value. The refinement converged to R = 4.64%, R_w = 5.32 (see Table 1). All software and the source of scattering factors are contained in the SHELXTL program library. Atom coordinates are given in Table 2 and selected bond distances and angles in Tables 3 and 4 respectively. An ORTEP drawing showing the molecular structure of $Zn(S_2CNEt_2)_2(TMEDA)$ is given in Figure 3. FIG. 3

(iv) Powder Generation and Characterization. A schematic diagram of the aerosol reactor is shown in Figure 4. The precursor was delivered into the reactor in solution as droplets suspended in a carrier gas. A solution of $Zn(S_2CNEt_2)_2(TMEDA)$ dissolved in toluene (10 mg/mL) was atomized using a modified Collison nebulizer. Nitrogen carrier gas was supplied to the Collison at 35 psig resulting in a carrier gas flow rate of 19.4 Lpm (at ambient conditions). The nitrogen gas carried the aerosol to a hot-wall reactor where the solvent and precursor evaporated and the precursor vapor then reacted to form ZnS particles. This approach provides a constant precursor delivery rate and keeps the precursor at room temperature until introduction into the reactor thereby avoiding problems associated with slow thermal decomposition of the precursor. This method has been used before for particle generation in plasma[34] and flame reactors,[35] and for CVD processes.[36-38] The small particle size of the resulting powder and the dependence of particle size on temperature indicated that the precursor evaporated and reacted in the gas phase.[17]

The reactor consisted of a mullite tube (3.25 inch I.D. X 60 inch length) contained

in a 3-zone, high-temperature furnace that had a 36 inch heated zone. A 147 mm Gelman stainless steel filter holder containing a nylon filter (pore size = 0.45 μm) was used for particle collection. Experiments were conducted holding all generation and collection variables constant while changing the reaction temperature. The precursor was reacted at temperatures of 500, 600, and 700 °C resulting in residence times of 5.8, 5.2 and 4.6 seconds, respectively.

The powders were characterized using x-ray diffraction (XRD), thermal gravimetric analysis (TGA), scanning electron micrograph (SEM), transmission electron micrograph (TEM), infrared spectroscopy (IR), elemental analysis (EA), and furnace atomic absorption (AA).

Results and Discussion

The use of single-source metal-organic precursors for the formation of binary materials has been the subject of much recent research,[18-26] especially for 3/5 materials such as GaAs and InP.[18,19,21,23,24]. For 2/6 materials, the metal dialkyldithiocarbamates are generally dimeric.[30-33] The de-oligomerization of metal-organic complexes in the presence of donor molecules is well known and has recently been used to facilitate isolation and crystallization of monomeric 2/6 precursors.[39] It is also well known that bidentate ligands that are capable of chelation are more likely to induce de-oligomerization relative to their monodentate counterparts, primarily for entropic reasons.[40] Here, the reaction between $[Zn(S_2CNEt_2)_2]_2$ and two equivalents of TMEDA resulted in isolation of a white crystalline solid according to Equation (1).

$$[Zn(S_2CNEt_2)_2]_2 + 2\ TMEDA \text{ ---> } 2\ Zn(S_2CNEt_2)_2(TMEDA) \qquad (1)$$

To examine the degree of oligomerization and the Zn coordination environment in this species in the solid state, a single-crystal X-ray diffraction study was carried out. An ORTEP plot is shown in Figure 3 and the relevant crystallographic parameters are presented in Tables 1-4. The $Zn(S_2CNEt_2)_2(TMEDA)$ is monomeric in the solid state with TABLES 1-4 a distorted octahedral Zn^{II} coordination environment. The Zn-S bonds in the dialkyldithiocarbamate groups are significantly longer (2.52 Å, average) than in $Zn(S_2CNEt_2)_2$ (2.38 Å, average), and the S-Zn-S bite angles are correspondingly smaller for $Zn(S_2CNEt_2)_2(TMEDA)$ (71.3°, average) compared to the dimer (75.5° average). The Zn-N distances are in the range expected based on the sum of their covalent radii and the TMEDA bite angle is 79.2°. In the solid-state infrared spectrum, the absorption at 1480 cm^{-1} was assigned to a C-N stretch frequency consistent with the C=N double bond character due to electron density delocalization among the CS_2^- group. Bands at 993 cm^{-1} and 567 cm^{-1} were assigned to asymmetric and symmetric C-S bond stretches, and the

absorption at 437 cm^{-1} was assigned to the Zn-S bond stretch. In the solid state this molecule exhibits approximately C_2 symmetry, and as a result two types of ethyl, methyl, and methylene groups are expected to be observed by ^1H and ^{13}C NMR spectroscopy in solution if this molecule is stereochemically rigid. However, at room temperature only one type of each of these groups was observed by ^1H NMR spectroscopy in C_6D_6 and C_7D_8 solution. On cooling a toluene-d_8 solution of $Zn(S_2CNEt_2)_2(TMEDA)$, all the ^1H NMR resonances broadened at ≈ 203 K, but the low-temperature limiting spectrum could not be reached due to the low activation barrier for this process. However, the methylene protons of the ethyl groups and the methyl groups on TMEDA showed splitting into two equal intensity resonances, consistent with the solid-state structure observed by X-ray diffraction. At this stage the remaining resonances (derived from TMEDA and S_2CNEt_2 methyl protons) were broad singlets probably as a result of their smaller chemical shift difference in the low-temperature limiting spectrum compared to the protons closer to the Zn center.

The origin of this dynamic exchange process is not clear at this stage, although we observed that the parent dimer $[Zn(S_2CNEt_2)_2]_2$ also undergoes a dynamic exchange process in toluene-d_8 solution with a significantly lower barrier. At room temperature a single set of ethyl group resonances was observed by ^1H and ^{13}C NMR spectroscopy which on cooling to 173 K only broadened slightly. These data are consistent with rapid bridge-terminal S_2CNEt_2 ligand exchange in the dimer, but the nature of this process (i.e., inter- vs. intra-molecular) was not established. The higher barrier in the case of $Zn(S_2CNEt_2)_2(TMEDA)$ is likely to be caused by removal of vacant coordination sites due to the presence of the TMEDA ligand. It is not possible to establish which ligand, i.e., TMEDA or S_2CNEt_2 is responsible for the exchange process from the data available. However, in analogous systems involving tertiary phosphine adducts of $Cd(S_2CNEt_2)_2$, the exchange process clearly involves cleavage of the Cd-P bond as determined by loss of the $^1J_{31P-111/113Cd}$ coupling at room temperature.[39] The relatively low solubility of

$Zn(S_2CNEt_2)_2(TMEDA)$ in benzene has precluded accurate molecular weight measurements to establish the degree of oligomerization in solution. These solution exchange phenomena are clearly important in connection with the use of these species as precursors for the formation of inorganic materials because such processes may have a profound influence on the decomposition behavior and vapor pressure.

The thermal decomposition of gaseous $Zn(S_2CNEt_2)_2(TMEDA)$ to form ZnS particles was examined in the hot-wall reactor. X-ray diffraction indicated that phase-pure wurtzite ZnS was formed at 500, 600, and 700 °C (Fig. 5). Peak widths in the 600 and 700 °C XRD patterns corresponded to 9 and 11 nm sized crystallites while at 500 °C the peaks were too broad to determine crystallite size. FIG 5.

Scanning electron micrographs (Fig. 6) revealed that the powders produced at 500, 600, and 700 °C consisted of 50, 40, and 30 nm particles, respectively, while 20 nm crystallites were observed by TEM of the 500 and 700 °C powders (Fig. 7). The discrepancies between particle size observed by SEM and crystallite size from XRD and TEM could be the result of formation of polycrystalline particles. A second reason could be the different sample preparation methods. Transmission electron micrograph samples were prepared by dispersing the particles in acetone, dipping a grid into the suspension, and allowing the grid to dry. In contrast, the SEM sample preparation used no liquid for dispersion. The acetone used during TEM sample preparation may have removed an outer coating of material from the particles, thereby reducing the apparent particle size. Crystallite size determinations of 10 nm from XRD line broadening are consistent with this hypothesis. FIG 6. FIG 7.

The possibility of a coating of a second material on the ZnS particles was examined in more detail. The motivation was to determine the origin of the differences in particle size discussed above, along with the possibility of gaining a better understanding of the mechanism of particle formation. Figure 8 is an illustration of the atomization and evaporation of the precursor followed by a possible reaction mechanism for particle FIG 8

formation. After reaction of the precursor, byproducts are liberated which can condense from the gas phase to coat the ZnS particles. In extreme cases, separate particles of the byproduct may be formed, although no evidence was observed for this.

Infrared spectroscopy of the powders showed the byproduct exhibited an absorbtion at 2100 cm^{-1}. No absorbance was observed in this region for the precursor, authentic ZnS, or S. The absorbance at this wavenumber is most likely attributed to $\nu(C\equiv N)$. The byproduct associated with the particles was extracted into acetone and after evaporation of the solvent a solid residue was obtained. Infrared spectroscopy showed this species contained the same IR band at 2100 cm^{-1} as found in the powders.

The identity of the byproduct was also investigated by elemental analysis and atomic absorption spectroscopy. The 600 °C sample gave analytical data of 5.65% C, 0.70% H, and 1.04% N, by weight. Furnace atomic absorption showed that the 600 °C sample was 50.4 wt% Zn. Assuming that all of the Zn in the sample is contained in ZnS, this corresponds to 75 wt% ZnS. Therefore, at least 25 wt % of the 600 °C sample was likely to be a byproduct. From EA, about 7.4 wt% of the sample was comprised of C, H, and N. Thus, the remaining 17.6 wt % was most likely sulfur. Therefore, the byproducts were probably a combination of elemental sulfur and a CN-containing species. The expected byproduct, Et-SCN, was not observed.

Summary and Conclusions

The feasibility of producing nanometer-sized ZnS aerosol particles by thermally decomposing a single-source, volatile precursor in the gas phase was demonstrated. This method is analogous to approaches for the preparation of films using single-source precursors and to liquid-phase approaches using similar precursors. A wide variety of volatile single-source precursors have been developed for CVD applications and should permit generation of a number of types of multicomponent particles by vapor phase routes. The impurities present in the ZnS powders are most likely derived from the $^-[S_2CNEt_2]$

ligands. This suggests that forming higher purity particles requires design of precursors in which ligand decomposition is better controlled to produce high vapor pressure products which do not condense on the particles either in the gas phase or on the filter.

Acknowlegments

We thank the UNM/NSF Center for MicroEngineered Ceramics and the Office of Navel Research for support of this work. Mark Hampden-Smith thanks NSF for the purchase of a low-field NMR spectrometer.

Supplementary Materials: X-ray crystallographic data for $Zn(S_2CNEt_2)_2(TMEDA)$, Structure Determination Summary, Bond Lengths and angles, Anisotropic Displacement Coefficients, H-Atom Coordinates and Isotropic Displacement Coefficients (14 pages), refinement summary, additional figures and observed and calculated structure factors (23 pages). Ordering information is given on any current masthead.

References

1. See e.g., "Frontiers in Materials Science", *Science* **1992**, *255*, 1049 and references therein.
2. Pool, R. *Science* **1990**, *248*, 1186, and references therein.
3. Marquardt, P.; Nimtz, G.; Muhlschlegel, B. *Solid State Communications* **1988**, *65*, 539.
4. Che, M.; Bennett, C.; "The Influence of Particle Size on the Catalytic Properties of Supported Metals", *Advances in Catalysis* **1989**, *36*, 55. Eley, D.; Pines, H.; Weiz, P. eds.; Academic Press, NY. See also Glassl, H.; Hayek, R.; Kramer, R.*J. Catal.* **1981**, *68*, 397.
5. Davis, S.; Klabunde, K. *Chem. Rev.* **1982**, *83*, 153.
6. Matijevic, E.; Garg, A. *Langmuir* **1988**, *4*, 26.
7. Brinker, C.; Scherer, G. *Sol-Gel Science, The Physics and Chemistry of Sol-Gel Processing*; Academic Press:, NY, 1990.
8. Riecke, R. *Science* **1989**, *246*, 1260; Riecke, R.; Burns, T.; Wehmeyer, R.; Kahn, B. in "High Energy Processes in Organometalic Chemistry", *ACS Symposium Series 333*; American Chemical Society: Washington, D.C., 1987.
9. Murthy, T.U.M.S.; Miyamoto, N.; Shimbo, M.; Nishizawa, J. *J. Cryst. Growth* **1976**, *33*, 1-7.
10. Okuyama, K.; Jeung, J.; Kousaka, Y.; Nguyen, H.; Jwang Wu, J.; Flagan, R. *Chem. Engr. Sci.* **1989**, *44*, 1369-75.
11. Okuyama, K.; Kousaka, Y.; Tohge, N.; Yamamoto, S.; Jwang Wu, J.; Flagan, R.; Seinfeld, J. *AIChE Journal* **1986**, *32*, 2010-19.
12. Wu, J.; Flagan, R.; Gregory, O. *Appl. Phys. Lett.* **1986**, *49*(2), 82-4.
13. Flagan, R.; Atwater, H.A.; Vahala, K.J. *J. Aerosol Sci.*, 1991, **22** (Suppl. 1), S31-S33.
14. Sercel, O.; Saunders, W.; Atwater, H.; Flagan, R. *Appl. Phys. Lett.* **1992**, *61*, 696-8.

15. Fujita, K.; Furukawa, Y.; Kaito, C. *J Crystal Growth*, **1985**, *71*, 821-3.

16. O'Brian, S.; Liu, Y.; Zhang, Q.; Heath, J.; Tittel, F.; Curl, R.; Smalley, R. *J. Chem. Phys.* **1986**, *84*,

17. Kodas, T. *Adv. Mater.* **1989**, *6*, 180-91.

18. Jones, R.A.; Cowley, A.H.; Benac, B.L.; Kidd, K.B.; Ekert, J.G.; Miller, J.E. *Mat. Res. Soc. Symp. Proc.* **1989**, *131*, 51-7.

19. Schulze, R.; Mantell, D.; Gladfelter, W.; Evans, J. *J. Vac. Sci. Technol. A* **1988**, *6*(3), 2162-3.

20. Aylett, B.; Tannahill, A. *Vacuum* **1985**, *35*(10-11), 435.

21. Amato, C.; Hudson, J.; Interrante, L. *Mat. Res. Soc. Symp. Proc.* **1991**, *204*, 135-40.

22. Fix, R.; Gordon, R.; Hoffman, D. *Chem. Mater.* **1990**, *2*, 235-41.

23. Interrante, L.; Lee, W.; McConnell, M.; Lewis, N.; Hall, E. *J. Electrochem. Soc.* **1989**, *136*(2), 472-78.

24. Jones, R.; Cowley, A.; Ekerdt, J. *Mat. Res. Soc. Symp. Proc.* **1991**, *204*, 73-81.

25. Liu, D.; Lai, A.; Chin, R. *Mat. Lett.* **1991**, *10*(7,8), 318-22.

26. Chiu, H.-T.; Chang, W.-P. *J. Mater. Sci. Lett.* **1992**, *11*, 96-8.

27. Armitage, D.; Yates, H.; Williams, J.; Cole-Hamilton, D.; Patterson, I. *Adv. Mater. for Optics and Electronics* **1992**, *1*, 43-6.

28. Ungarish, M. *Proceedings of the Sixth Eur. Conf. on CVD*, Mar. to Apr., 1987, 32-40.

29. Frigo, D.; Khan, O.; O'Brien, P. *J Crystalline Growth* **1989**, *96*, 989.

30. Hursthouse, M.B.; Malik, M.A.; Motivalli, M.; O'Brien, P. *Organometallics* **1991**, *10*, 730.

31. Malik, M.A.; O'Brien, P. *Chem. Mater.*, **1991**, *3*, 999.

32. Malik, M.A.; Motevalli, M.; Walsh, J.R.; O'Brien, P. *Organometallics*, 1991, 11, 3136.

33. O'Brien, P. in *Inorganic Materials*, Chapt. 9; Bruce, D.W.; O'Hare, D.; eds.; Wiley:

Chichester, 1992, and references therein.

34. Kagawa, M.; Honda, F.; Onodera, H.; Nagae, T. *Mat. Res. Bull.*, **1983**, *18*, 1081-87.

35. Sokolowski, M.; Sokolowsda, A.; Michalski, A.; Gokieli, B. *J. Aerosol Sci.* **1977**, *8*, 219-30.

36. Salazar, K.; Ott, K.; Dye, R.; Hubbard, K.; Peterson, E.; Coulter, J.; Kodas, T. *Physica C*, **1992**, *198*, 303-8.

37. Lambeck, P.V.; Hilderink, L.; Popma, Th.J.A. *Proc. S&A Symp. of the Twente Univer. of Tech.*, Oct. 30-31, 1986, 85-95.

38. Siefert, W. *Thin Solid Films* **1984**, *121*, 275-82.

39. Zeng, D.; Hampden-Smith, M.J.; Rheingold, A.; Alam, T. *Inorg. Chem.*, submitted, 1993.

40. Shriver, D.F.; Atkins, P.W.; Langford, C.H. in *Inorganic Chemistry*; W.H. Freeman and Co: New York, 1990.

Figure Captions

Figure 1. Gas-phase reaction of two precursors leading to formation of particles with composition that varies from particle to particle and within individual particles.

Figure 2. Gas-phase reaction of single-source precursor leading to formationm of particles with uniform composition..

Figure 3. ORTEP plot of $Zn(S_2CNEt_2)_2(TMEDA)$

Figure 4. Hot-wall reactor used for gas-phase particle formation.

Figure 5. X-ray diffraction patterns of ZnS produced at a) 500 °C, b) 600 °C, and c) 700 °C.

Figure 6. Scanning electron micrographs of ZnS produced at a) 500 °C, b) 600 °C, and c) 700 °C.

Figure 7. Transmission electron micrographs ZnS produced at a) 500 °C, and b) 700 °C.

Figure 8. Reaction mechanism in which both ZnS and by product condense from gas phase.

Table 1. Summary of Crystallographic Data for $Zn(S_2CNEt_2)_2(TMEDA)$

chemical formula	$C_{16}H_{36}N_4S_4Zn$
formula weight	478.1
space group	$P2_12_12_1$
a, Å	8.785 (1)
b, Å	11.611 (2)
c, Å	23.321 (2)
V, Å^3	2378.9 (6)
Z	4
T, °C	20
λ, Å	0.71073
ρ_{calcd}, g cm^{-3}	1.335
μ, cm^{-1}	12.93
$R(F_o)$[a], %	4.64
$R_W(F_o)$[b], %	5.32

[a] $R(F_o) = \Sigma(|F_o| - |F_c|)/\Sigma|F_o|$

[b] $R_W(F_o) = S(w^{1/2}(|F_o| - |F_c|))/(w^{1/2}|F_o|)$; $w^{-1} = s^2(F_o) + 0.0061F_o^2$

Table 2. Atomic coordinates ($x10^4$) and equivalent isotropic displacement coefficients ($Å^2x10^3$) for $Zn(S_2CNEt_2)_2(TMEDA)$

	x	y	z	U(eq)
Zn	1326 (1)	4851 (1)	8531 (1)	39 (1)
S(1)	1368 (2)	2693 (1)	8690 (1)	42 (1)
S(2)	-83 (3)	4417 (1)	9435 (1)	55 (1)
S(3)	1414 (2)	7005 (1)	8671 (1)	50 (1)
S(4)	3835 (2)	5383 (1)	8990 (1)	56 (1)
N(1)	116 (7)	2192 (5)	9706 (2)	42 (2)
C(1)	427 (7)	3008 (5)	9316 (3)	36 (2)
C(2)	-596 (8)	2423 (6)	10257 (3)	43 (2)
C(3)	533 (11)	2571 (8)	10725 (3)	77 (4)
C(4)	513 (9)	972 (5)	9606 (3)	54 (3)
C(5)	-812 (9)	325 (7)	9352 (3)	66 (3)
N(2)	3819 (7)	7605 (5)	9286 (2)	51 (2)
C(6)	3126 (8)	6765 (6)	9008 (3)	40 (2)
C(7)	3276 (9)	8787 (6)	9281 (3)	54 (3)
C(8)	3779 (11)	9458 (7)	8769 (4)	77 (3)
C(9)	5271 (9)	7375 (7)	9609 (3)	61 (3)
C(10)	6598 (14)	7661 (12)	9292 (6)	130 (6)
N(3)	-769 (6)	4869 (5)	7945 (2)	51 (2)
N(4)	2456 (7)	4693 (6)	7649 (2)	55 (2)
C(11)	-146 (13)	5020 (12)	7363 (4)	107 (5)
C(12)	1270 (12)	4400 (10)	7263 (4)	93 (4)
C(13)	-1761 (12)	5862 (8)	8071 (6)	119 (6)
C(14)	-1666 (14)	3873 (9)	7996 (5)	99 (5)
C(15)	3638 (12)	3764 (7)	7642 (4)	77 (3)
C(16)	3244 (13)	5765 (8)	7487 (4)	85 (4)

*Equivalent isotropic U defined as one third of the trace of the orthogonalized U_{ij} tensor

Table 3. Bond lengths (Å) for $Zn(S_2CNEt_2)_2(TMEDA)$

Zn-S(1)	2.533 (2)	Zn-S(2)	2.494 (2)
Zn-S(3)	2.524 (2)	Zn-S(4)	2.526 (2)
Zn-N(3)	2.293 (5)	Zn-N(4)	2.293 (6)
S(1)-C(1)	1.716 (6)	S(2)-C(1)	1.719 (6)
S(3)-C(6)	1.719 (7)	S(4)-C(6)	1.722 (7)
N(1)-C(1)	1.342 (8)	N(1)-C(2)	1.455 (8)
N(1)-C(4)	1.477 (8)	C(2)-C(3)	1.485 (11)
N(2)-C(7)	1.453 (9)	C(4)-C(5)	1.506 (11)
C(7)-C(8)	1.494 (12)	N(2)-C(6)	1.320 (9)
C(9)-C(10)	1.420 (15)	N(2)-C(9)	1.505 (10)
N(3)-C(11)	1.473 (11)	N(3)-C(13)	1.476 (12)
N(3)-C(14)	1.404 (12)	N(4)-C(12)	1.418 (12)
N(4)-C(15)	1.497 (11)	N(4)-C(16)	1.474 (11)
C(11)-C(12)	1.457 (17)		

Table 4. Bond angles (°) for $Zn(S_2CNEt_2)_2(TMEDA)$

S(1)-Zn-S(2)	71.6 (1)	S(1)-Zn-S(3)	164.0 (1)
S(2)-Zn-S(3)	96.1 (1)	S(1)-Zn-S(4)	99.6 (1)
S(2)-Zn-S(4)	97.2 (1)	S(3)-Zn-S(4)	71.1 (1)
S(1)-Zn-N(3)	96.2 (2)	S(2)-Zn-N(3)	96.2 (1)
S(3)-Zn-N(3)	95.3 (2)	S(4)-Zn-N(3)	161.9 (2)
S(1)-Zn-N(4)	92.6 (2)	S(2)-Zn-N(4)	163.1 (2)
S(3)-Zn-N(4)	100.5 (2)	S(4)-Zn-N(4)	91.3 (2)
N(3)-Zn-N(4)	79.2 (2)	Zn-S(1)-C(1)	84.6 (2)
Zn-S(2)-C(1)	85.8 (2)	Zn-S(3)-C(6)	85.7 (2)
Zn-S(4)-C(6)	85.5 (2)	C(1)-N(1)-C(2)	123.9 (5)
C(1)-N(1)-C(4)	121.4 (5)	C(2)-N(1)-C(4)	114.7 (5)
S(1)-C(1)-S(2)	117.8 (3)	S(1)-C(1)-N(1)	121.6 (5)
S(2)-C(1)-N(1)	120.6 (5)	C(6)-N(2)-C(7)	122.8 (6)
N(1)-C(2)-C(3)	112.5 (6)	C(7)-N(2)-C(9)	116.7 (6)
N(1)-C(4)-C(5)	111.0 (6)	S(3)-C(6)-N(2)	120.5 (5)
C(6)-N(2)-C(9)	120.4 (6)	Zn-N(3)-C(11)	104.6 (5)
S(3)-C(6)-S(4)	117.2 (4)	C(11)-N(3)-C(13)	108.0 (8)
S(4)-C(6)-N(2)	122.2 (5)	C(11)-N(3)-C(14)	112.6 (8)
N(2)-C(7)-C(8)	113.8 (6)	Zn-N(4)-C(12)	105.7 (5)
N(2)-C(9)-C(10)	113.2 (8)	C(12)-N(4)-C(15)	109.3 (7)
Zn-N(3)-C(13)	111.2 (6)	C(12)-N(4)-C(16)	112.7 (7)
Zn-N(3)-C(14)	113.1 (6)	N(3)-C(11)-C(12)	114.0 (9)
C(13)-N(3)-C(14)	107.2 (7)	N(4)-C(12)-C(11)	114.0 (8)
Zn-N(4)-C(15)	111.5 (5)	C(15)-N(4)-C(16)	106.3 (7)
Zn-N(4)-C(16)	111.5 (5)		

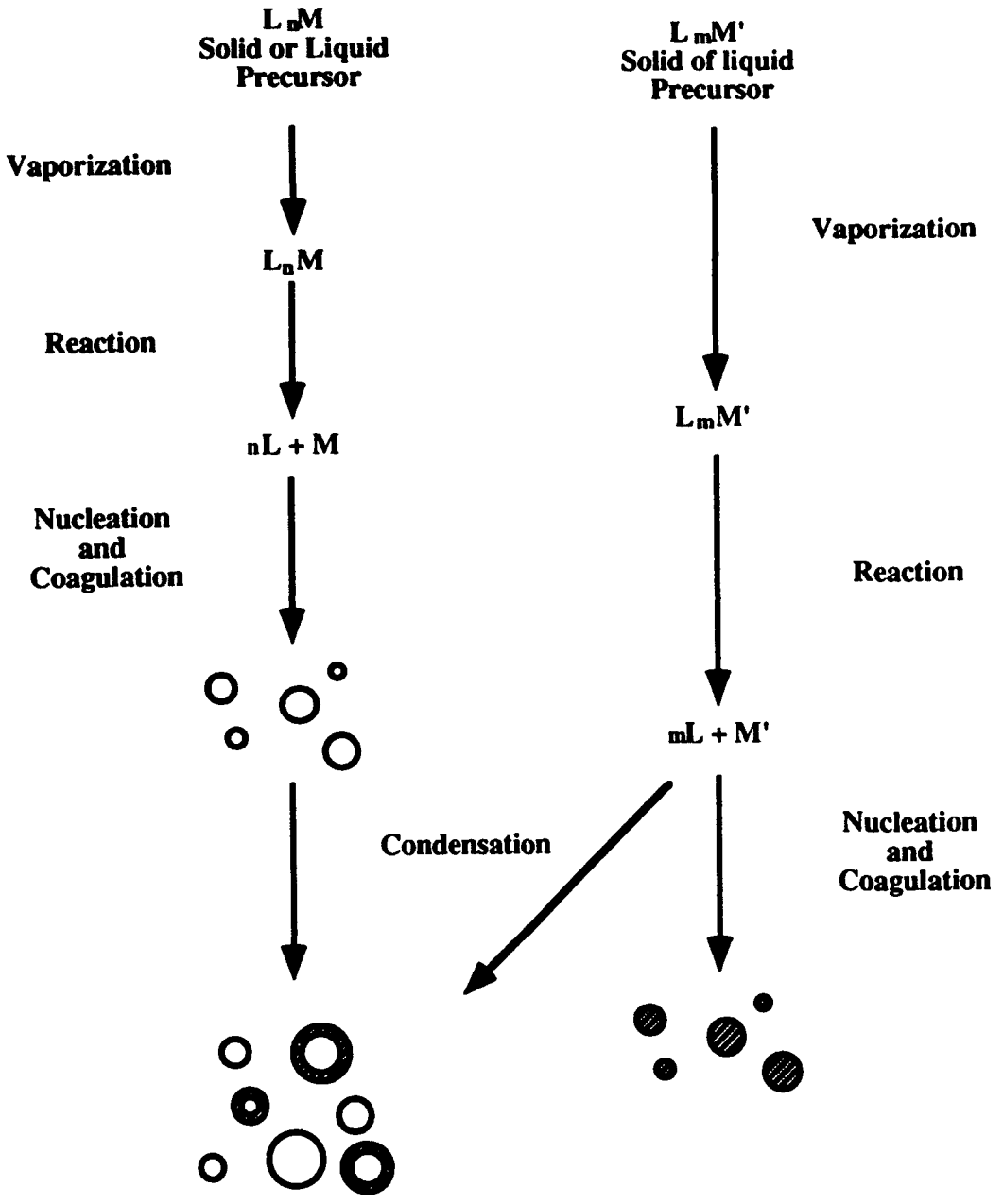
L_nM
Solid or Liquid
Precursor
L_mM'
Solid of liquid
Precursor
Vaporization
L_nM
Vaporization
Reaction
L_mM'
$nL + M$
Nucleation
and
Coagulation
Reaction
$mL + M'$
Condensation
Nucleation
and
Coagulation

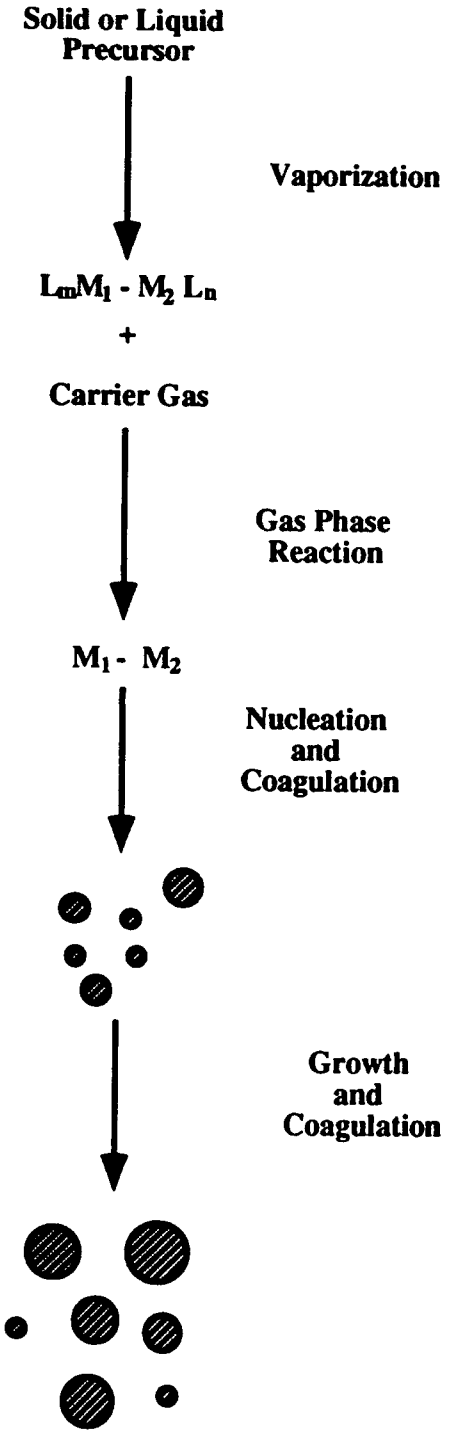
Solid or Liquid Precursor
Vaporization
$L_mM_1 - M_2 L_n$
+
Carrier Gas
Gas Phase Reaction
$M_1 - M_2$
Nucleation and Coagulation
Growth and Coagulation

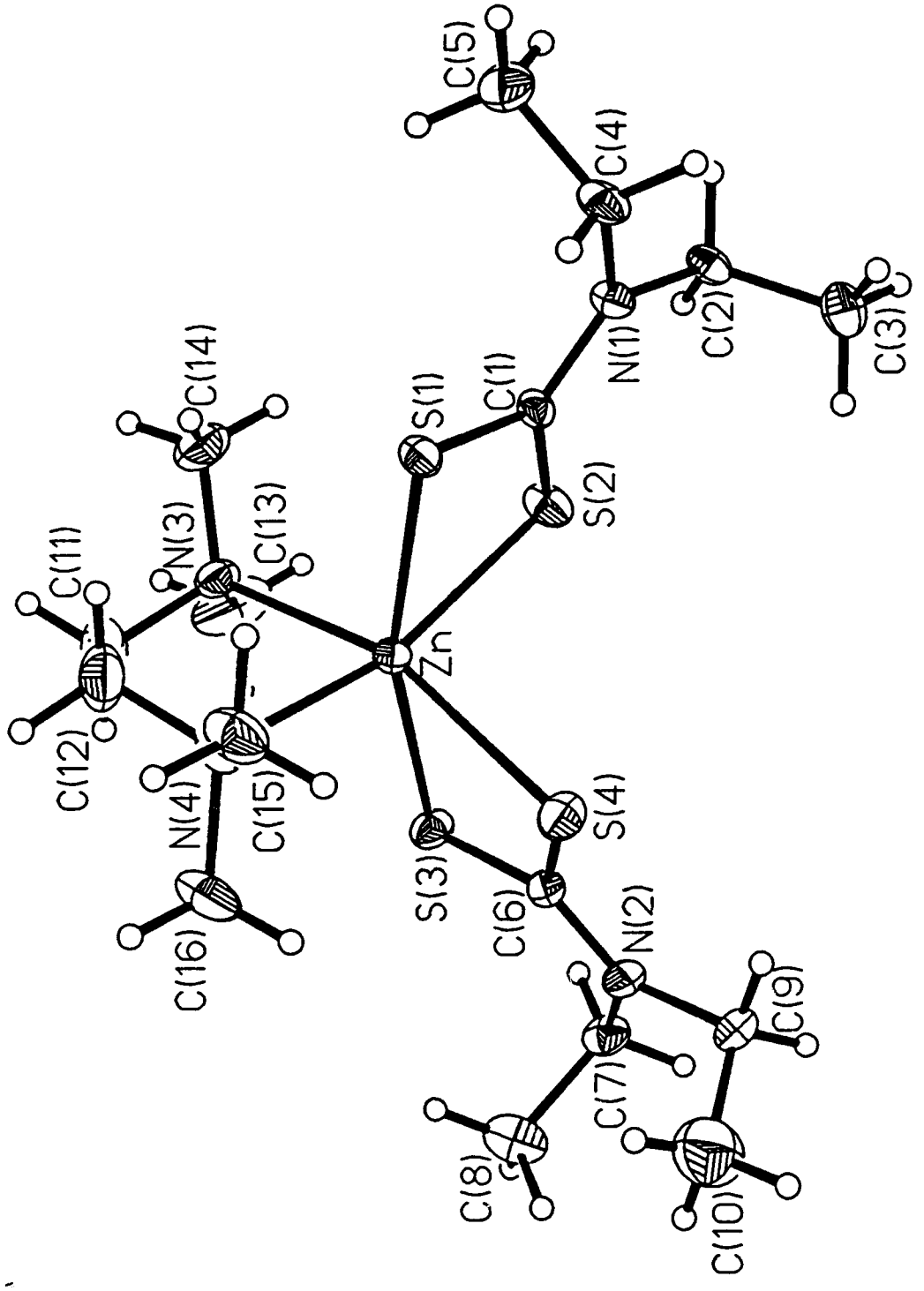
C(5)
C(4)
N(1)
C(2)
C(3)
S(1)
C(1)
S(2)
C(14)
N(3)
C(13)
C(11)
Zn
C(12)
N(4)
C(15)
C(16)
S(3)
S(4)
C(6)
N(2)
C(9)
C(7)
C(8)
C(10)

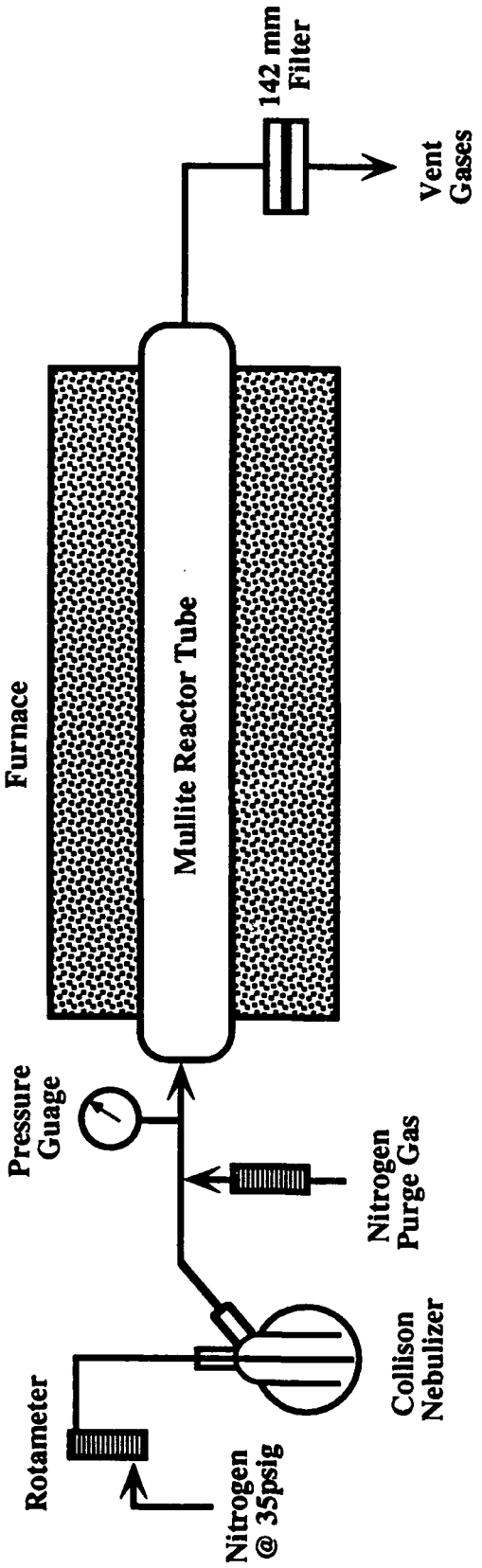
142 mm
Filter
Vent
Gases
Furnace
Mullite Reactor Tube
Pressure
Guage
Nitrogen
Purge Gas
Collison
Nebulizer
Rotameter
Nitrogen
@ 35psig

5

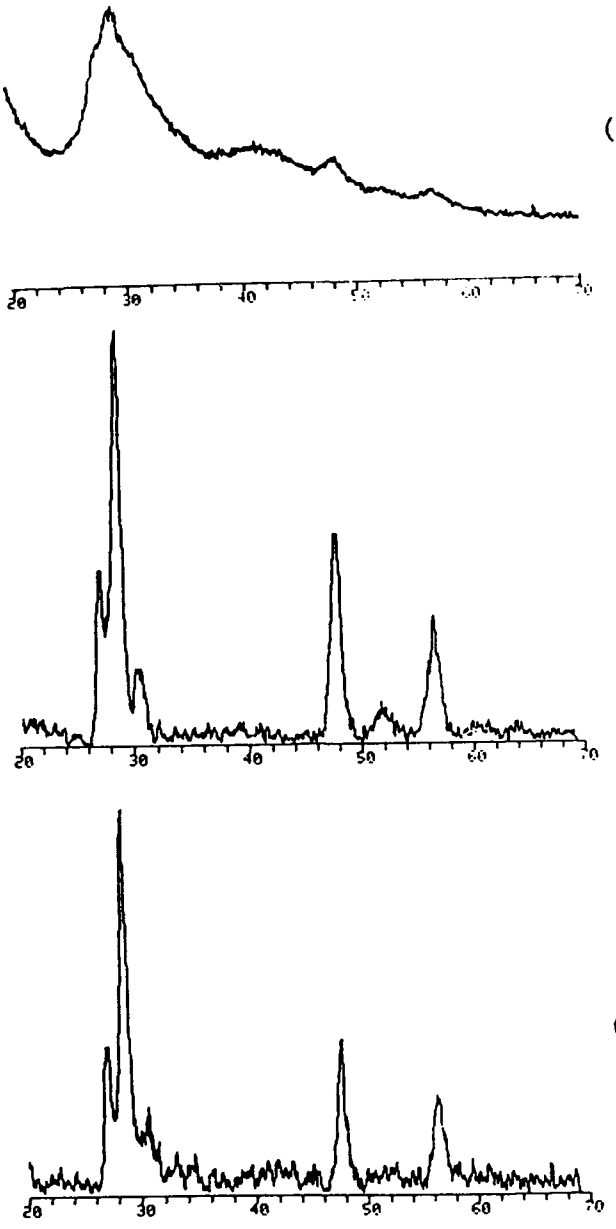

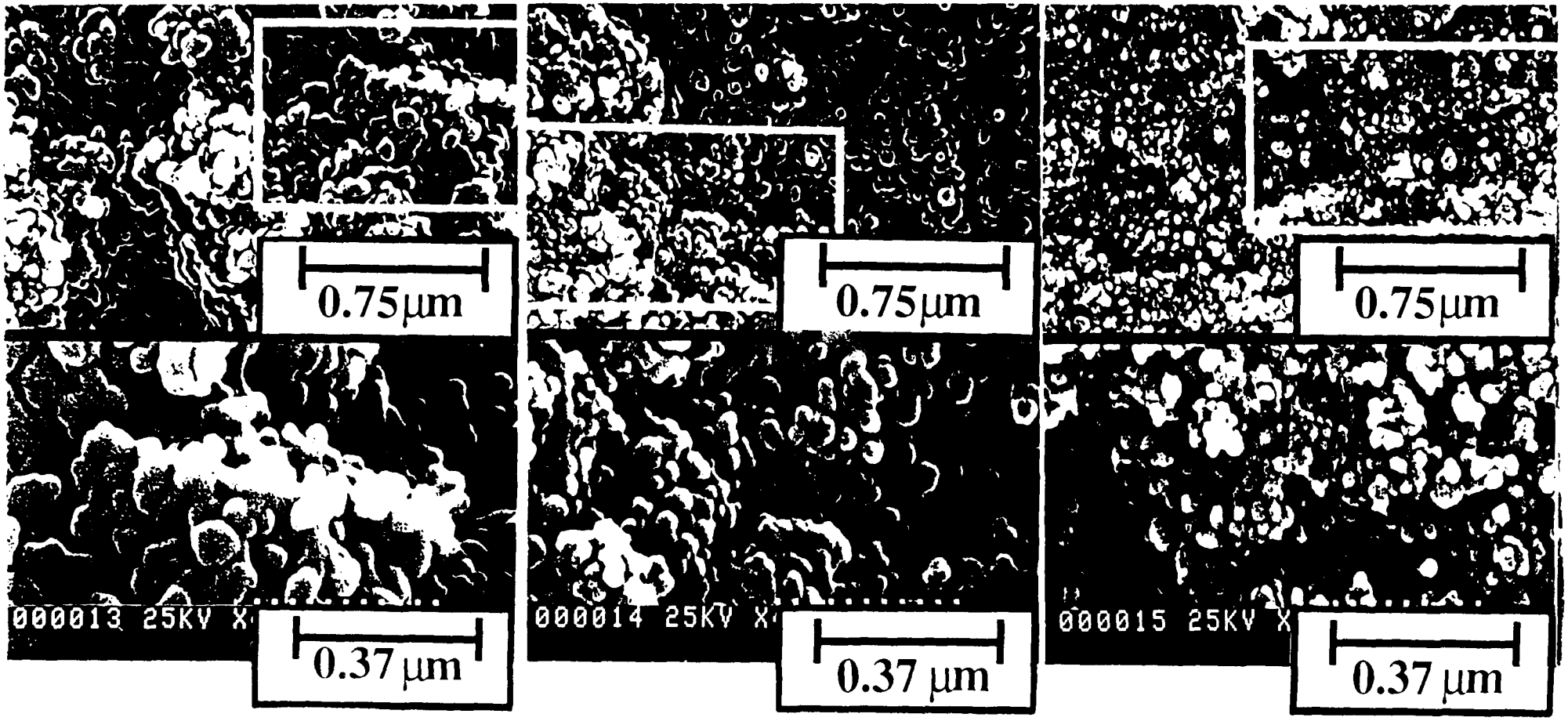
0.75μm
000013 25KV X
0.37 μm
0.75μm
000014 25KV X
0.37 μm
0.75μm
000015 25KV X
0.37 μm

(a) (b) (c)

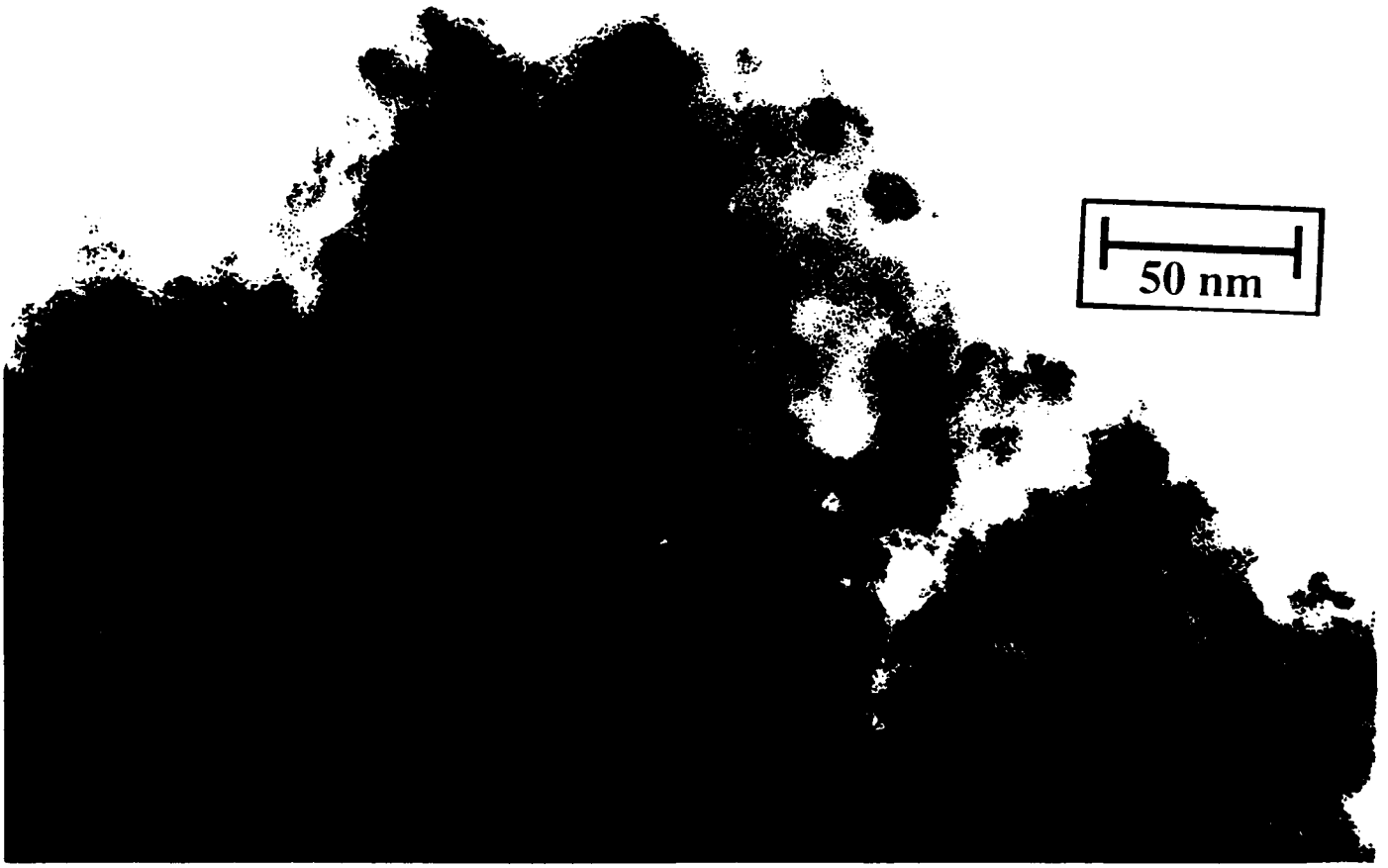
50 nm

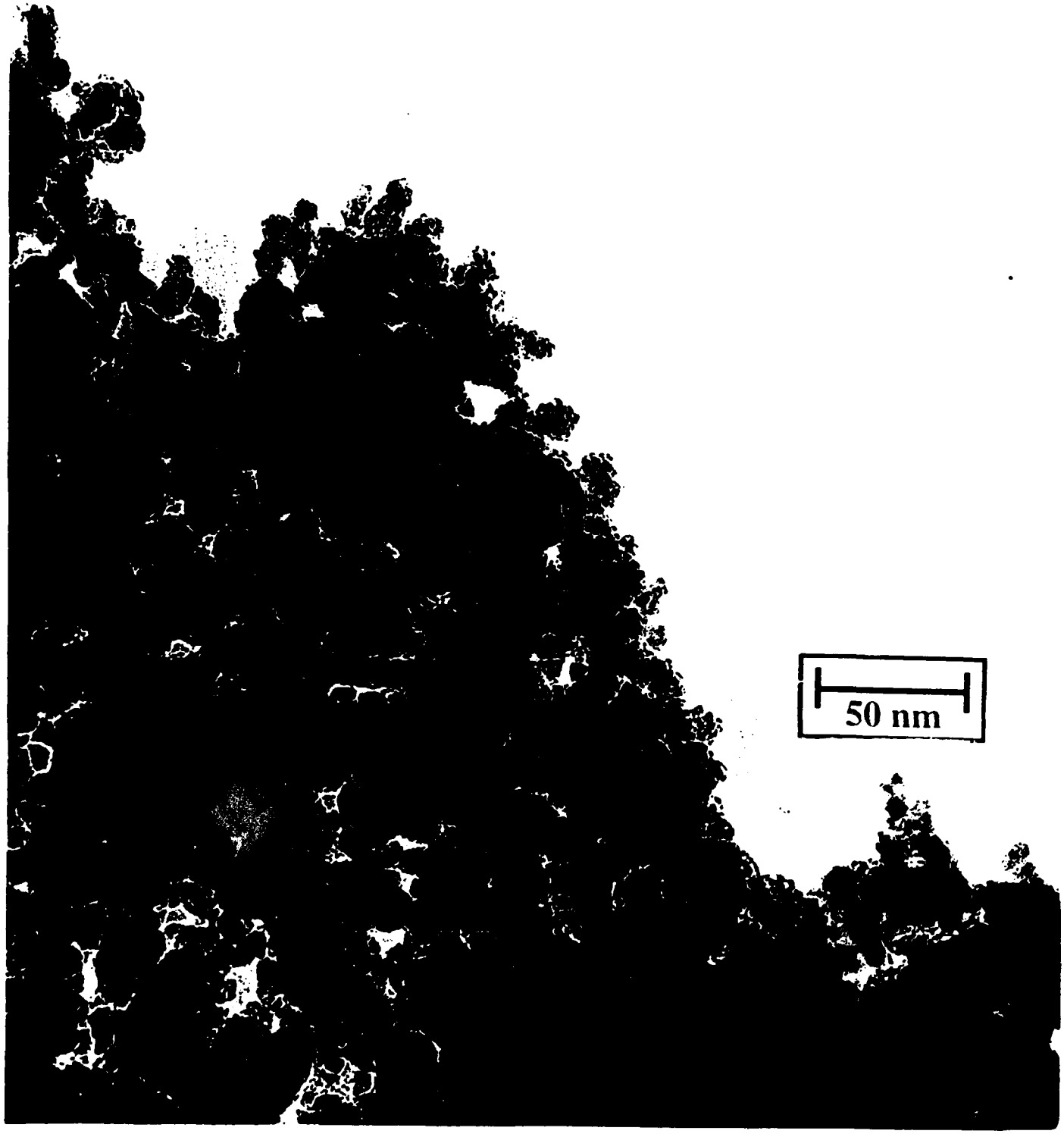
50 nm

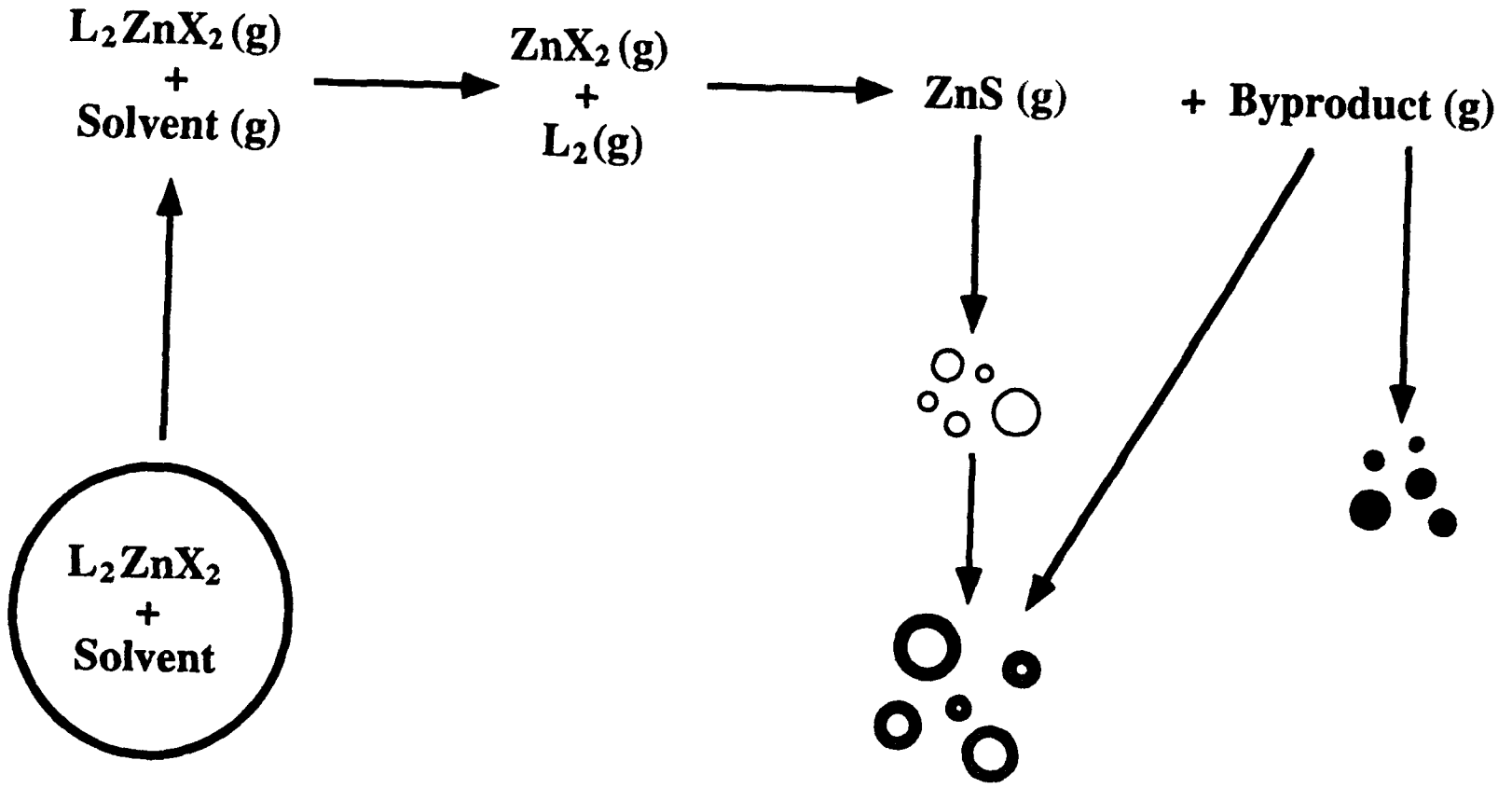

L_2 = TMEDA
X = S_2CNEt_2